Int. J. Electrochem. Sci., 17 **(2022)** Article Number: 220669, doi: 10.20964/2022.06.65

International Journal of
ELECTROCHEMICAL
SCIENCE
www.electrochemsci.org

Facile in Situ Fabrication of a Co-Fe Bimetallic N-doped Carbon Xerogel as an Efficient Electrocatalyst for Oxygen Reduction Reaction in Acidic and Alkaline Media

Ling Pi[1], *Hong Jin*[2,*], *Laihong Zhou*[3], *Hongke Pan*[1]

[1] School of Architectural Engineering, Xinyu University, Xinyu, Jiangxi, 338004, China
[2] School of New Energy Science and Engineering, Xinyu University, Xinyu, Jiangxi, 338004, China
[3] School of Mechanical and Electrical Engineering, Xinyu University, Xinyu, Jiangxi, 338004, China
[*]E-mail: hjin00@126.com

Received: 26 February 2022 / *Accepted:* 12 April 2022 / *Published:* 7 May 2022

Nitrogen-doped carbon xerogels (NCX) have been used as non-precious metal electrocatalysts for oxygen reduction reaction (ORR). In this study, a Co-Fe bimetallic nitrogen-doped carbon xerogel (CoFeNCX) electrocatalyst with high contents of quaternary N and pyridinic N and a uniformly distributed bimetallic structure was prepared by facile sol-gel and pyrolysis methods. The resulting materials were characterized by scanning electron microscopy, field-emission transmission electron microscopy, energy-dispersive spectrometry, and X-ray photoelectron spectroscopy. Electrochemical testing of the catalyst by using a thin-film rotating disk electrode revealed its superior performance in acidic and alkaline electrolytes. The ORR performance of the bimetallic CoFeNCX electrocatalyst was remarkably better than those of CoNCX and FeNCX materials, which was primarily attributed to the high proportions of quaternary N and pyridinic N in the CoFeNCX electrocatalyst. The non-precious metal catalysts developed herein can be used as an efficient electrocatalyst for ORR in acidic and alkaline membrane fuel cells.

Keywords: N-doped carbon xerogel; oxygen reduction reaction; electrocatalyst; alkaline and acidic media

1. INTRODUCTION

Increase in energy consumption and depletion of traditional fossil fuels have resulted in a series of global energy crisis and environmental pollution. Therefore, there is an urgent need to develop clean, renewable, and efficient alternative energy systems to meet the energy supply requirements of humans.[1,2] Fuel cell technology has attracted increasing attention due to its high-power density and low environmental impact. Thus far, platinum-based electrocatalysts are still the most effective

electrocatalysts for oxygen reduction reaction (ORR). However, the high costs and poor long-term stability of Pt seriously hinder large-scale applications of fuel cells. Therefore, the development of novel, highly active, and low-cost non-precious metal catalysts (NPMC) and their application as alternatives to platinum-based electrocatalysts are of immense importance to promote the commercialization of fuel cells.[3-5] Transition metals have been reported to promote the bonding of nitrogen atoms in a carbon six-membered carbon ring, forming a more active nitrogen–carbon structure with high-edge exposure.[6,7] The nature of carbon networks plays a key role in ORR. The addition of nitrogen atoms into the carbon structure significantly increases ORR activity because it enhances the electron density of materials and their abilities to contribute electrons. In addition, delocalization induced by nitrogen doping can improve oxygen adsorption, thereby promoting ORR. The morphology, structure, electronic characteristics, and composition of carbon carriers used for the synthesis of N-doped carbon materials exert key effects on the types and number of different N species in the final materials, thereby affecting the electrocatalytic performance in ORR.[8-11] Various N-doped carbon materials, such as carbon nanotubes, graphite, ordered mesoporous carbon, graphite, and carbon nanofibers, etc., have been used as electrocatalysts for ORR. Among these materials, carbon xerogels (CXs) continue to attract considerable attention mainly because of their competitive price and adjustable surface chemical states.[12-15] Material synthesis is simple, and facile scale-up is possible. In addition, new materials with a high porosity, high specific surface area, and high pore size distribution can be obtained by the simple adjustment of the synthetic parameters. In fact, the presence of medium-to-large pores in CX structures facilitates mass transfer in ORR. Currently, a carbon gel is mainly used as the carrier of precious metals, precious-metal alloys, or transition metals (such as Co, Fe, Ni).[16-19] Previously, our group has investigated the effect of cobalt metal (Co) on the ORR activity of a nitrogen-doped CX in acidic and alkaline media.[20,21] The results reveal that the catalyst exhibits a good catalytic activity as well as stability. Fe–N–C is well known to exhibit excellent ORR activity, while Co–N–C exhibits good durability. Therefore, to further increase the density of the active center in nitrogen-doped carbon xerogels (NCX) and catalytic ORR performance, a series of novel Co-Fe bimetallic nitrogen-doped carbon xerogel (CoFeNCX) electrocatalysts were developed by simple sol-gel and pyrolysis methods. In addition, factors affecting the performance of the CoFeNCX catalyst were investigated via the optimization of the composition and treatment temperature. The ORR electrocatalytic activity of the prepared materials in acidic and alkaline media was evaluated on an electrochemical workstation. High contents of pyridine nitrogen and graphite nitrogen in CoFeNCX rendered better ORR catalytic activity and stability than those of pure cobalt and ferroelectric catalysts.

2. EXPERIMENTAL

2.1. Catalyst preparation

First, the resorcinol formaldehyde Co-Fe (RFCoFe) xerogel was prepared by the polymerization of resorcinol, formaldehyde, cobalt acetate, and ferric nitrate; then the RFCoFe xerogel was functionalized by N doping in ammonia to afford a CoFeNCX composite electrocatalyst. The RFCoFe

precursor system was prepared as follows: First, 6.16 g (0.056 mol) of resorcinol ($C_6H_6O_2$, AR) was dissolved in 7.0 mL of deionized water, and a cobalt acetate solution ($Co(CH_3COO)_2{\cdot}4H_2O$, AR) was slowly added to the solution and stirred until it was completely dissolved. Next, a $Fe(NO_3)_3$ solution ($Fe(NO_3)_3{\cdot}9H_2O$, AR, R:Co:Fe molar ratio = 40:1:1) was added to the solution, and stirring was continued until the solid was completely dissolved. Subsequently, 9.08 g (0.112 mol) of a formaldehyde solution (HCHO, AR, 37 wt%, Tianjin Damao Chemical Reagent Factory) was dropped, followed by the slow addition of ammonia water (NH_3, 25–28 wt%, AR, Xilong Chemical Co., LTD.) to the solution for a reaction to form a hydrogel. Then, the organic hydrogels were transferred to a vacuum drying oven for vacuum drying and closed aging at 85°C for 7 days, affording RFCoFe organic xerogel precursor samples. After the sample was crushed, it was heat-treated at 800°C in ammonia for 2 h and then naturally reduced to room temperature, affording a Co-Fe bimetallic composite N-doped CoFeNCX electrocatalyst. To compare the effect of CoFe doping, the same preparation method was employed to prepare samples with Co:Fe molar ratios of 1:0, 5:1, 2:1, 1:1, 1:2, 1:5, and 0:1.

2.2. Materials characterization

Sample morphologies were analyzed on a JEOL JSM 6701F field-emission scanning electron microscopy (FE-SEM) system. A Philips CM-1 X-ray diffractometer was utilized to investigate the bulk phase structure of the samples under the following test conditions: Cu Kα1 radiation source (λ = 1.54056 A), a tube voltage of 20 kV, and a scanning range of 20°–80°. Field-emission transmission electron microscopy (FE-TEM) and energy-dispersive spectrometry (EDS) measurements were conducted on a Talos F200X system to observe catalyst morphology. X-ray photoelectron spectroscopy (XPS) data were recorded on an Axis Ultra DLD spectrometer and with a mono Al K α X-ray source (Al mono, 150 W). The C1s (284.6 eV) peak was selected as the internal standard. Deconvolution of the XPS peak was conducted by an XPS peak fitting program (XPSPEAK Version 4.1).

2.3. Electrochemical measurements

Electrochemical performance of the catalysts was measured by cyclic voltammetry (CV) and using a conventional three-electrode system on a PGSTAT302N electrochemical workstation (Metrohm Corp., Switzerland). The working electrode was prepared as follows: First, 5 mg of the catalyst sample, 1 mL of ethanol, and 50 μL of a 5 wt% Nafion solution were mixed by ultrasonication, affording a uniform slurry. Second, 10 μL of the slurry was extracted and transferred to a glassy carbon electrode with an area of 0.19625 cm^2. After drying at room temperature, a thin-film electrode was formed. The total amount of the catalyst sample on the electrode was 0.2426 $mgcm^{-2}$. The reference and counter electrodes were a saturated KCl calomel electrode (SCE, potential of 0.242 V relative to the standard hydrogen electrode RHE) and Pt wire electrode, respectively, and the electrolyte was 0.5 $molL^{-1}$ H_2SO_4 solution or 0.1 $molL^{-1}$ KOH solution. Unless otherwise noted, the electrode potential in CV was relative to RHE. High-purity N_2 was continuously pumped into the electrolyte for 30 min before the test at room

temperature to remove the dissolved oxygen from the solution. The potential scanning range was 0–1.2V, and the scanning rate was 100 mVs^{-1}.

The catalyst activity in ORR was measured using a rotating disc electrode (RDE) on the PGSTAT302N electrochemical workstation with a rotary unit (PINE Corp., USA). The test conditions and environment were the same as those used in the CV test, and oxygen was allowed to flow into the electrolyte for 30 min before the test to saturate it with oxygen. The scanning range was from 1.2 V to 0.0 V, scanning rate was 5 mVs^{-1}, and electrode speed was 1600 rpm. Catalyst stability was evaluated by an accelerated aging test (AAT) based on continuous potential cycling for 1000 cycles at room temperature. The AAT was conducted by scanning the potential between 0 and 1.2 V at a scan rate of 50 mVs^{-1} in a 0.5 M H_2SO_4 electrolyte purged with N_2. The ORR performances (before and after AAT) were investigated by RDE measurements using the same standard three-electrode electrochemical system as described above. The electrolyte was saturated by O_2, and the ORR polarization curve was recorded at a rotating speed of 1600 rpm.

3. RESULTS AND DISCUSSION

3.1 Physical characterization of catalysts

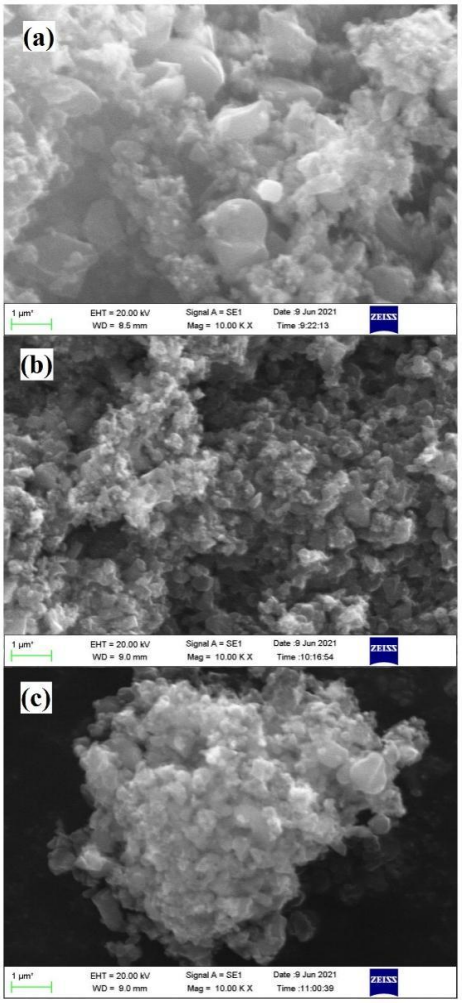

Figure 1. Scanning electron micrographs of samples (a) CoFeNCX (b) CoNCX and (c) FeNCX.

As can be observed from the SEM images of (a) CoFeNCX, (b) CoNCX, and (c) FeNCX samples in Figure 1, the three samples exhibit microgranular and evenly distributed surface morphologies. CoNCX samples are more evenly distributed, while FeNCX samples are slightly agglomerated. The distribution state of the CoFeNCX sample is between those of the CoNCX and FeNCX samples.

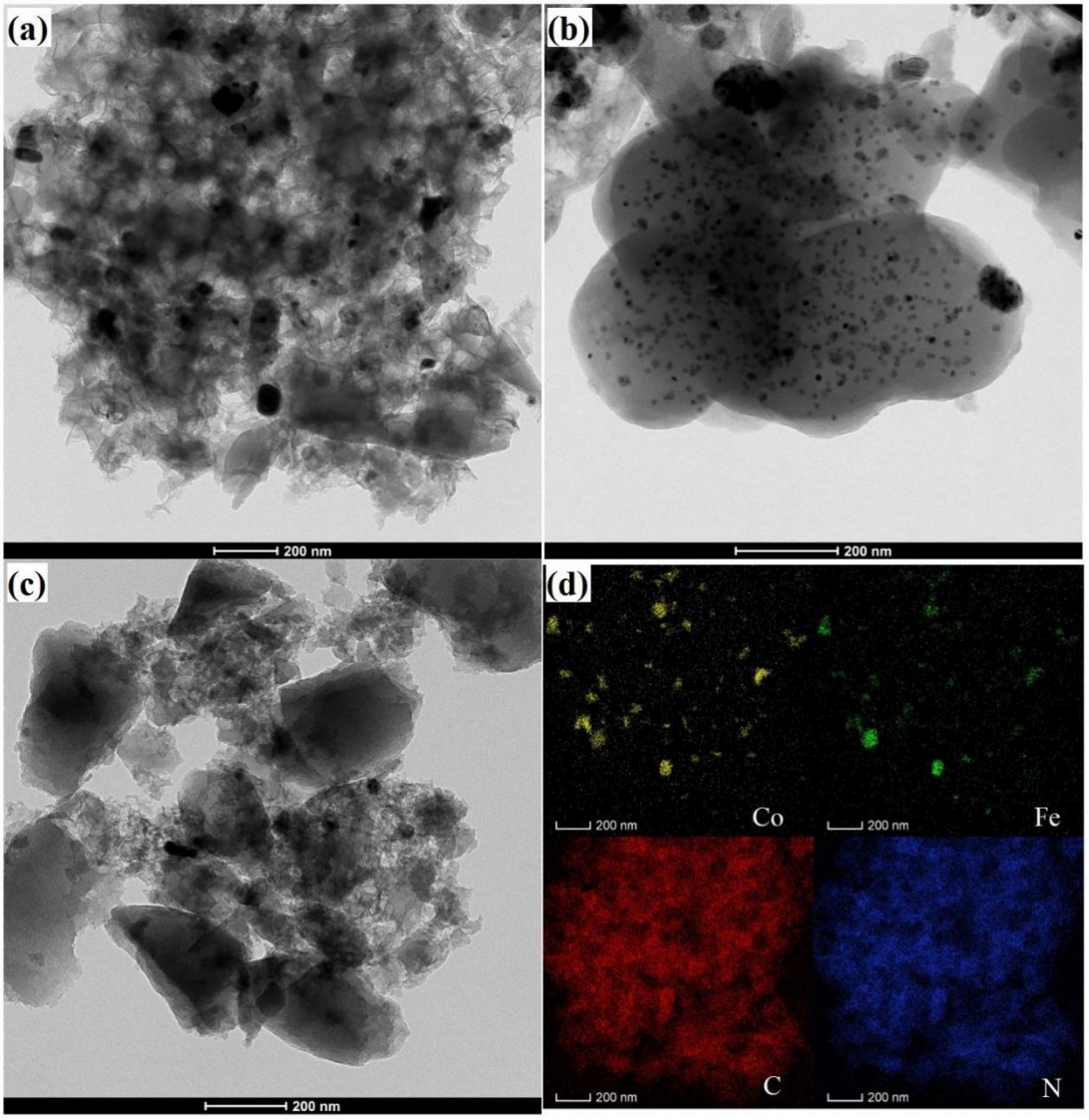

Figure 2. FE-TEM pictures (a) CoFeNCX (b) CoNCX and (c) FeNCX. (d) The elemental mapping image of CoFeNCX sample.

To further investigate the microstructure of the prepared catalyst, FE-TEM was employed to analyze the microstructure and composition of the sample (Figure 2). Figures 2 (a), (b), and (c) shows the FE-TEM images of CoFeNCX, CoNCX, and FeNCX catalyst samples, respectively. The comparison of the CoNCX sample reveals carbon nanospheres with a uniform distribution of metal particles on the surface, while the FeNCX sample exhibits an irregular and considerable carbon distribution, with a low amount of dispersed metal particles. Compared with the distributions of CoNCX and FeNCX, the microcosmic distribution of CoFeNCX is more uniform, showing irregular, amorphous carbon

distribution, and surface doping leads to relatively uniform metal particles. The elemental mapping image reveals that the distributions of Co and Fe are basically consistent, the distributions of C and N are consistent, and the doping of N is relatively uniform. FE-TEM analysis reveals that the prepared bimetal-doped NCX catalyst exhibits a more uniform microstructure and element composition than those of the single-metal doped NCX catalyst. This uniform structure contributes to the better catalytic activity of the material in the electrocatalytic process.[22-24]

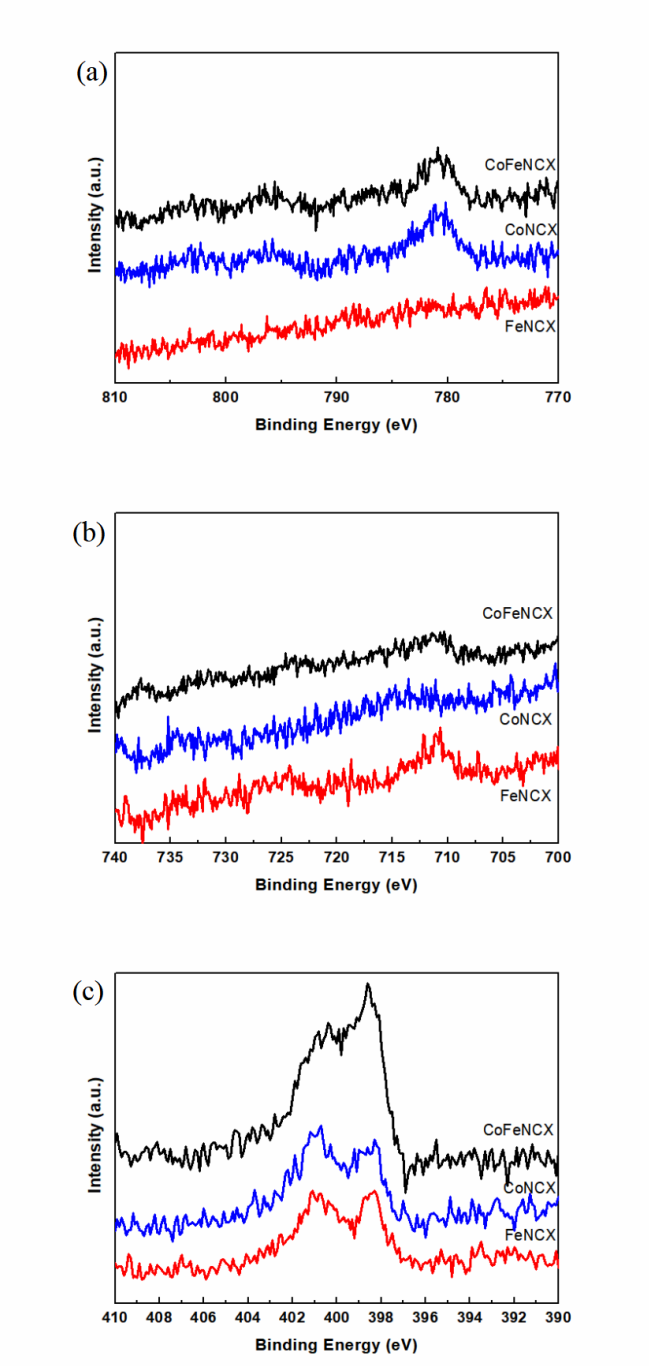

Figure 3. XPS spectra of CoFeNCX, CoNCX and FeNCX samples (a) Co 2p (b) Fe 2p and (c) N 1s.

XPS was employed to analyze the surface chemical states of CoFeNCX, CoNCX, and FeNCX materials. The peak at 775–870 eV corresponds to the satellite peaks of Co2p (Figure 3 (a)).[25,26] Compared to the FeNCX samples, CoFeNCX and CoNCX samples exhibit a clear Co2p spectrum.

The peak at 705–735 eV in Figure 3(b) corresponds to the satellite peaks of Fe2p.[27] Compared to CoNCX samples, CoFeNCX and FeNCX samples exhibit a clear Fe2p spectrum. The peak observed at 394–408 eV corresponds to satellite peaks of N1s.[28,29] CoFeNCX, CoNCX, and FeNCX samples exhibit a clear N1s spectrum. However, compared with those of the CoNCX and FeNCX samples, the N1s peak of CoFeNCX sample is clearer, and the peak area is higher, indicating that the N doping content of the CoFeNCX sample is higher. Table 1 shows the atom content according to the XPS C1s, N1s, O1s, Co2p, and Fe2p region analysis of CoFeNCX, CoNCX, and FeNCX samples.

Table 1. Overview of the XPS C1s, N1s, O1s, Co2p and Fe2p region analysis of CoFeNCX, CoNCX and FeNCX (atom contents).

Sample ID	C 1s (%)	N 1s (%)	O 1s (%)	Co 2p (%)	Fe 2p (%)
CoFeNCX	82.04	1.02	16.76	0.09	0.09
CoNCX	81.25	0.72	17.91	0.13	--
FeNCX	80.07	0.56	19.30	--	0.07

According to the data listed in Table 1, the C and O contents did not change considerably in the CoFeNCX, CoNCX, and FeNCX catalysts. The content of N in CoFeNCX is 1.42 times of that in CoNCX and 1.82 times of that in FeNCX. Bimetal doping significantly improves the N content of the CoFeNCX catalyst. In addition, XPS analysis results also reveal that the doping amounts of Co and Fe in the CoFeNCX sample are the same (0.09%).

Table 2. Overview of the XPS N1s regions analysis of CoFeNCX, CoNCX and FeNCX samples.

Sample ID	pyridinic N-O		quaternary N		pyrrolic N		pyridinic N	
	B.E. (eV)	N (%)	B.E. (eV)	N (%)	B.E. (eV)	N (%)	B.E. (eV)	N (%)
CoFeNCX	403.5	10.18	401.0	44.85	399.7	14.32	398.4	30.65
CoNCX	403.1	18.03	401.0	42.23	399.5	16.59	398.4	23.15
FeNCX	402.8	18.30	401.0	34.62	399.8	13.22	398.4	33.87

In this study, chemical states of N in CoFeNCX, CoNCX, and FeNCX samples were further analyzed by the peak-splitting fitting method (Figure 4).

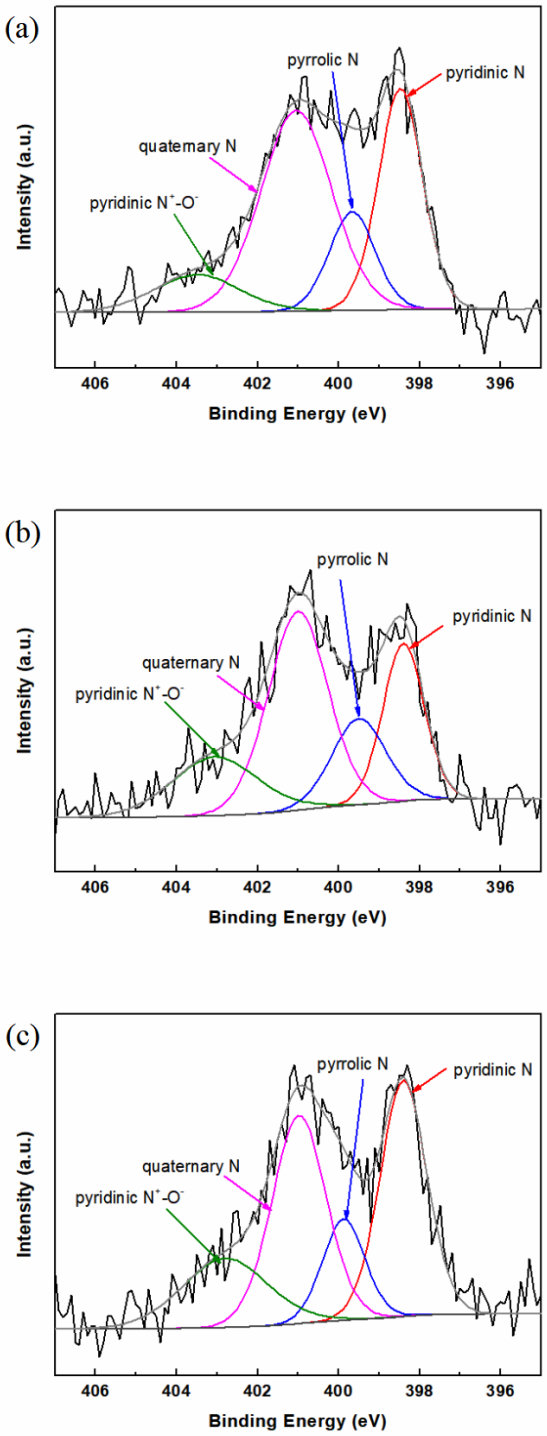

Figure 4. High-resolution XPS spectra N1s of the CoFeNCX, CoNCX and FeNCX samples.

Generally, N1s high-resolution spectra can be fitted into four peaks, corresponding to pyridinic N-O (402.8–403.5 eV), pyrrolic N (399.5–400.0 eV), and pyridinic N (397.6–398.4eV). Among them, the quaternary N and pyridinic N are thought to help catalyze ORR.[28-30] Table 2 shows the contents of the four chemical states of N calculated according to their peak areas after the peak fitting of

CoFeNCX, CoNCX, and FeNCX samples. As can be observed from the data shown in Table 2, the sum of the contents of quaternary N and pyridinic N in the CoFeNCX sample is the highest (75.50%); it is 1.15 times that of the CoNCX sample (65.38%) and 1.10 times that of the FeNCX sample. The CoFeNCX sample composition is beneficial to its catalytic ORR process.

3.2 Catalyst activity and stability

To confirm the catalytic performance of the prepared materials, the ORR activity of the catalysts in acidic and alkaline media was tested and analyzed on an electrochemical workstation using CV and linear sweep voltammogram (LSV) methods. Figures 5(a) and (b) show the electrochemical test results of samples with different proportions in the acidic electrolyte.

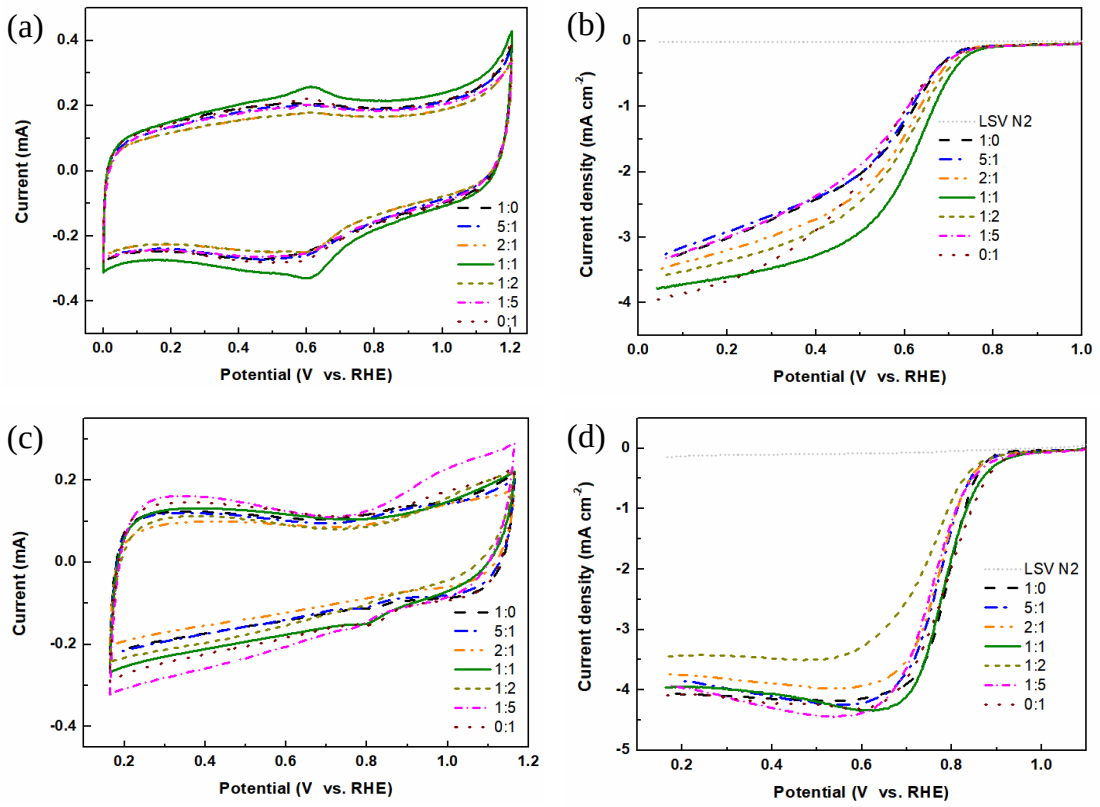

Figure 5. CV curves and LSV curves for Co_xFe_yNCX catalysts with Co:Fe=1:0, 5:1, 2:1, 1:1, 1:2, 1:5 and 0:1in (a,b) 0.5 $molL^{-1}$ H_2SO_4 electrolyte and (c,d) 0.1 $molL^{-1}$ KOH electrolyte.

As can be observed from the CV curves of the samples in Figure 5 (a), the CV curves of several samples exhibit nearly symmetrical rectangles, indicating that the samples exhibit good double-layer capacitance. The sample with a Co:Fe ratio of 1:1 exhibits the highest area enclosed by CV, indicating that the double-layer capacitance of the sample is the highest and that the electrochemical energy storage of the material is excellent. As can be observed from Figure 5(b), with the change in the doping ratio, the ORR performance of the material also gradually changes. Compared with those of samples with Co:Fe ratios of 1:0 and 0:1, the catalytic activity of the CoFeNCX sample with a Co:Fe ratio of 1:1 is

significantly improved. The initial oxygen reduction potential and half-wave potential are significantly greater than those of CoNCX and FeNCX samples. In an acidic electrolyte, a bimetal-doped CoFeNCX catalyst exhibits excellent ORR catalytic activity, which is consistent with XPS analysis results. Figure 5(c and d) shows the electrochemical test results of samples in different mol ratios in an alkaline electrolyte. As can be observed from the CV curves of the samples in Figure 5 (c), the CV diagrams of several samples are similar to those in the acidic electrolyte, with nearly symmetrical rectangles up and down, indicating that the samples exhibit good double-layer capacitance. As can be observed from Figure 5(d), with the change in the doping ratio, the ORR performance of the material also changes gradually, but the change range is small, and the change is slightly different from that observed in the acidic system. Compared to the samples with Co:Fe ratios of 1:0 and 0:1, the CoFeNCX sample with a Co:Fe ratio of 1:1 does not exhibit any clear advantage in terms of the catalytic activity. The initial ORR potential and half-wave potential are not different from those of CoNCX and FeNCX samples. In general, CoFeNCX samples exhibit good catalytic performance for ORR in acidic and alkaline electrolytes, which is possibly attributed to the high contents of quaternary N and pyridinic N in CoFeNCX samples, and the electrochemical test results further confirm the analysis conclusion of XPS.

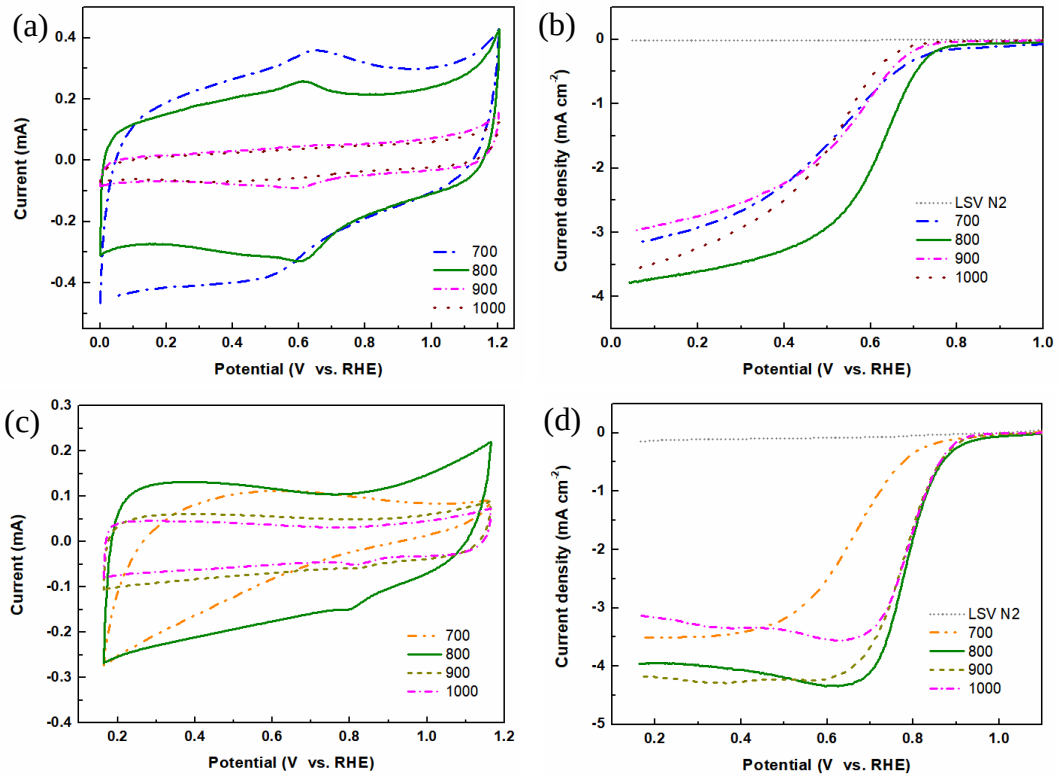

Figure 6. CV curves and LSV curves of CoFeNCX catalysts at pyrolysis temperature of 700, 800, 900 and 1000 ºC in a (a,b) 0.5 molL^{-1} H_2SO_4 electrolyte and (c,d) 0.1 molL^{-1} KOH electrolyte.

Next, the effect of pyrolysis temperature on catalytic activity was investigated. Figure 6 shows the comparison of CV and LSV curves of the CoFeNCX catalyst obtained by pyrolysis at different temperatures in acidic and alkaline media. As can be observed from the CV curve of the sample in Figure 6 (a), with the increase in the pyrolysis temperature, the electric double layer of the sample gradually

decreases. Pyrolysis temperatures considerably affect the capacitance performance of the catalyst. Among them, compared to the samples prepared at other temperatures, the CoFeNCX catalyst prepared at 700 °C exhibits better double-layer capacitance performance. As can be observed from the LSV curve of the sample in Figure 6 (b), the catalytic activity of the sample increases first and then decreases with the increase in the treatment temperature, and the CoFeNCX catalyst prepared at 800°C exhibits the best catalytic performance. The test results under alkaline conditions are slightly different from those under acidic conditions (Figure 6(c and d)). The CoFeNCX catalyst prepared at 800 °C exhibits the best double-layer capacitance performance (Figure 6 (c)). The catalytic properties of samples prepared at 700 °C, 800 °C, and 900 °C are similar(Figure 6 (d)). Considering the factors of the initial voltage, half-wave potential, and limiting current, the CoFeNCX catalyst prepared at 800 °C exhibits the best performance. Therefore, the CoFeNCX catalyst prepared at 800 °C exhibits better catalytic ORR performance both in acidic and alkaline electrolytes.

To investigate the possibility of the CoFeNCX catalyst replacing commercial Pt/C, LSV curves of the CoFeNCX catalyst were recorded and compared with that of the Pt/C catalyst in acidic and alkaline systems respectively (Figure 7). As can be observed from Figure 7 (a) and (b), the initial ORR potentials of the CoFeNCX catalyst are 0.832 V and 0.981 V, and the corresponding differences between commercial Pt/C (0.878 V and 0.990 V) are 0.046 V and 0.009 V. The half-wave potentials of the CoFeNCX catalyst are 0.612 V and 0.795 V, corresponding to differences of 46 mV and 51 mV from those of commercial Pt/C (0.658 V and 0.846 V), respectively. The initial ORR potentials and half-wave potentials of the CoFeNCX catalyst are comparable to those of cobalt and iron co-doped carbon catalysts, especially in acidic media. That is, for the (Co,Fe)-CN/RGO catalyst (onset potentials is 41 mV more negative than that of a commercial Pt/C) [31], for the FeCo@N-C/KB catalyst (the onset potential and half-wave potential are 100 mV and 80 mV less than those of Pt/C) [32] and Co_2/Fe-N@CHC catalyst (half-wave potential is 23 mV less than that of Pt/C)[33]. The performance of the CoFeNCX catalyst is still slightly far less than that of commercial Pt/C. However, the material and preparation costs of the CoFeNCX catalyst, as a cost-effective and facile method to prepare a non-noble metal catalyst, is considerably less than those of the Pt/C catalyst. Therefore, the CoFeNCX catalyst can be considered as a promising new catalyst to replace commercial Pt/C.

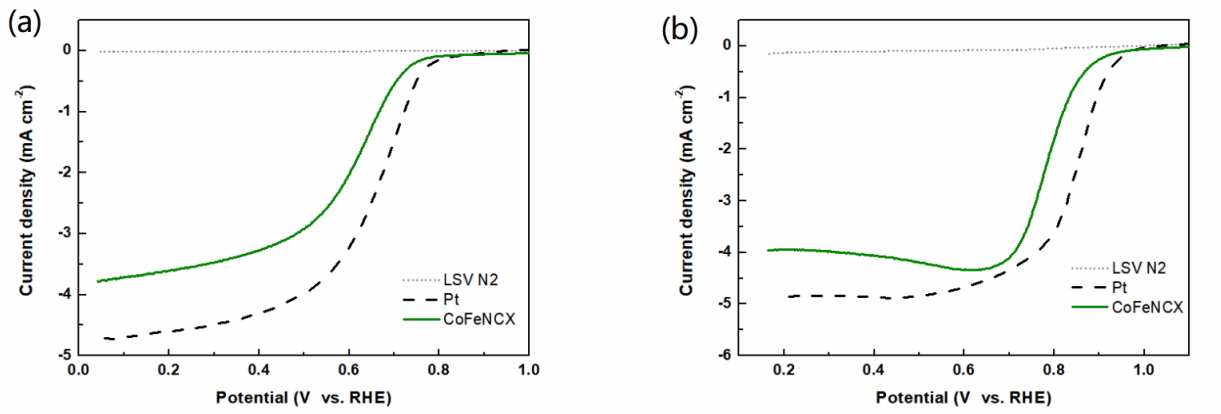

Figure 7. LSV curves of the CoFeNCX and Pt/C catalysts in (a) 0.5 molL^{-1} H_2SO_4 and (b) 0.1 molL^{-1} KOH electrolytes.

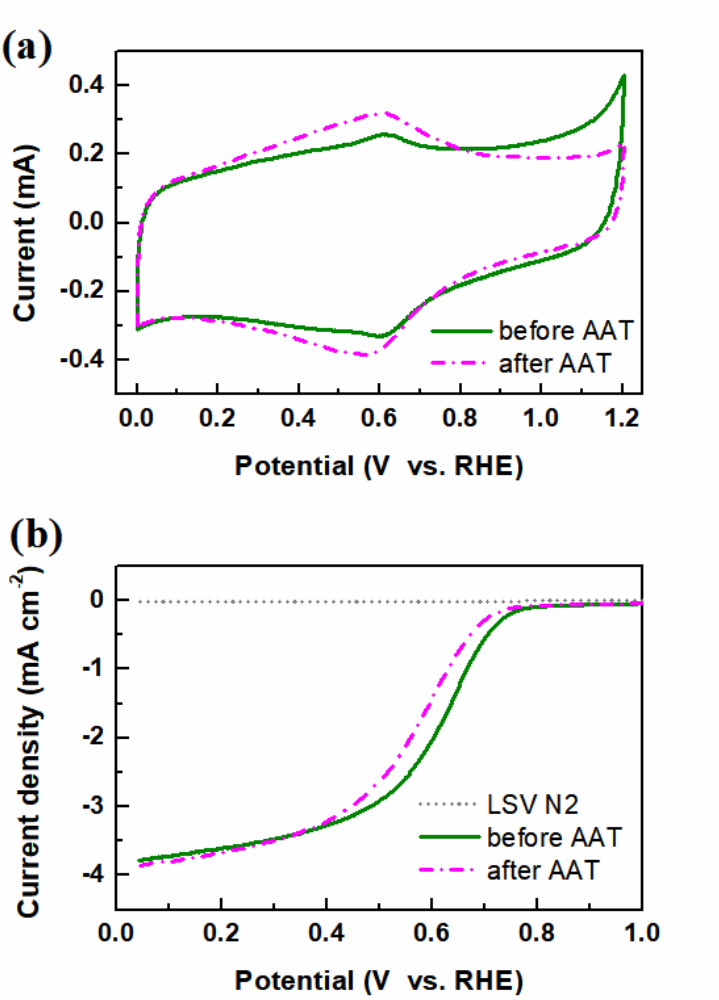

Figure 8. CV and LSV curves of the CoFeNCX catalyst before and after AAT in 0.5 $molL^{-1}$ H_2SO_4 electrolyte.

To investigate the stability of the catalyst in practical applications, the AAT method was employed to examine the stability of CoFeNCX. Figure 8 shows the results. As can be observed from Figure 8(a), before and after AAT, CV curves of samples reveal a double-electric layer structure with upper and lower symmetry and a small shape change, indicating that the CoFeNCX sample structure remains relatively stable after the AAT test. Figure 8(b) shows LSV curves of samples before and after AAT. As can be observed from the figure, after AAT, the initial ORR potential and half-wave potential of CoFeNCX samples are 0.803 V and 0.566 V, which are 29 mV and 46 mV less than those before AAT (0.832 V and 0.612 V), respectively. AAT does not lead to a significant potential drop. The CoFeNCX samples exhibit good electrochemical stability and excellent comprehensive performance, and these catalysts demonstrate immense promise to replace noble-metal catalysts in fuel cell applications.

4. CONCLUSIONS

In conclusion, a highly effective and low-cost FeCoNCX electrocatalyst is developed by a facile method for ORR in acidic and alkaline electrolytes. The high contents of quaternary N and pyridinic N can anchor high content of Co and Fe species, generating highly efficient active sites. Therefore, the FeCoNCX electrocatalyst exhibits outstanding activity and stability for ORR. This study provides novel insights into the design and synthesis of various non-precious carbon-based materials as efficient electrocatalysts for green energy storage and conversion technologies in the future.

ACKNOWLEDGEMENTS
The authors gratefully acknowledge the financial support by the Science & Technology Project of Education Department of Jiangxi Province, China (GJJ191060, GJJ212316, GJJ212320) and Science & Technology Guidance Plan Project of Xinyu City (21KJZD01, 21KJZD02).

References

1. S. Chu, A. Majumdar, *Nature*, 488 (2012) 294.
2. B. Dunn, H. Kamath, J.M. Tarascon, *Science*, 334 (2011) 928.
3. S.G. Peera, T.G. Lee, A.K. Sahu, *Sustainable Energy Fuels,* 3 (2019) 1866.
4. J. Tang, J. Liu, N.L. Torad, T. Kimura, Y. Yamauchi, *Nano Today*, 9 (2014) 305.
5. X. Zhou, J. Qiao, L. Yang, J. Zhang, *Adv. Energy Mater.*, 4 (2014) 1.
6. S. Liu, Z. Wang, S. Zhou, F. Yu, M. Yu, C.Y. Chiang, W. Zhou, J. Zhao, J. Qiu, *Adv. Mater.*, 29 (2017) 1.
7. E.J. Biddinger, U.S. Ozkan, *J. Phys. Chem. C*, 114 (2010) 15306.
8. H. Zhang, H. Osgood, X. Xie, Y. Shao, W. Gang, *Nano Energy*, 31 (2017) 331.
9. J. Frédéric, L. Michel, D. Jean-Pol, C. Mei, *J. Phys. Chem. B*, 110 (2006) 5553.
10. D. Guo, R. Shibuya, C. Akiba, S. Saji, T. Kondo, J. Nakamura, *Science* 351 (2016) 361.
11. K.H. Wu, D.W. Wang, D.S. Su, I.R. Gentle, *ChemSusChem*, 8 (2015) 2772.
12. H.C. Chang, C. Baldizzone, G. Polymeros, E. Pizzutilo, F. Jaouen, *ACS Catal.*, 6 (2016)3136.
13. A. Abidin, K.S. Loh, W.Y. Wong, A.B. Mohamad, I. Puspasari, *Int. J. Hydrogen Energy*, 43 (2018) 11047.
14. D. Geng, Y. Chen, Y. Chen, Y. Li, R. Li, X. Sun, S. Ye, S. Knights, *Energy Environ. Sci.*, 4 (2011) 760.
15. C. Chen, X. Zhang, Z.-Y. Zhou, X.-D. Yang, X.-S. Zhang, S.-G. Sun, *Electrochim. Acta*, 222 (2016) 1922.
16. A.F. Zainul Abidin, K.S. Loh, W.Y. Wong, A.B. Mohamad, *Int. J. Hydrogen Energy*, 44 (2019) 28789.
17. M. Canal-Rodríguez, N. Rey-Raap, J.Á. Menéndez, M.A. Montes-Morán, J.L. Figueiredo, M.F.R. Pereira, A. Arenillas, *Microporous Mesoporous Mater.*, 293 (2020) 109811.
18. Y. Wei, S. Chen, W. Lin, *Int. J. Hydrogen Energy*, 37 (2012) 942.
19. S. Liu, C. Deng, L. Yao, H. Zhong, H. Zhang, *J. Power Sources*, 269 (2014) 225.
20. H. Jin, H. Zhang, H. Zhong, J. Zhang, *Energy Environ. Sci.*, 4 (2011) 3389.
21. H. Jin, J. Li, F. Chen, L. Gao, H. Zhang, D. Liu, Q. Liu, *Electrochim. Acta*, 222 (2016) 438.
22. X. Jin, Y. Xie, L. Wang, J. Huang, *ChemElectroChem*, 7 (2020) 865.
23. M. Zhang, Y. Song, H. Tao, C. Yan, J. Masa, Y. Liu, X. Shi, S. Liu, X. Zhang, Z. Sun, *Sustainable Energy Fuels*, 2 (2018) 1820.
24. A. Sarapuu, L. Samolberg, K. Kreek, M. Koel, L. Matisen, K. Tammeveski, *J. Electroanal. Chem.*

746 (2015) 9.
25. Xiaojuan, Chen, Ming, Cheng, Di, Chen, Rongming, Wang, *ACS Appl. Mater. Interfaces*, 8 (2016) 3892.
26. G. Zhang, C. Li, J. Liu, L. Zhou, R. Liu, X. Han, H. Huang, H. Hu, Y. Liu, Z. Kang, *J. Mater. Chem. A*, 2 (2014) 8184.
27. E. Luo, C. Wang, Y. Li, X. Wang, L. Gong, T. Zhao, Z. Jin, J. Ge, C. Liu, W. Xing, *Nano Res.*, 13 (2020) 2420.
28. C. Guo, Y. Li, Y. Xu, Q. Xiang, L. Sun, W. Zhang, W. Li, Y. Si, Z. Luo, *Nanoscale Res. Lett.*, 14 (2019) 22.
29. R.G. Morais, N. Rey-Raap, R.S. Costa, C. Pereira, A. Guedes, J.L. Figueiredo, M.F. R. Pereira, *J. Compos. Sci.*, 4 (2020)1.
30. N.P. Subramanian, X. Li, V. Nallathambi, S.P. Kumaraguru, H. Colon-Mercado, G. Wu, J.-W. Lee, B.N. Popov, *J. Power Sources*, 188 (2009) 38.
31. W.-K. Jo, S. Moru, D.-E. Lee, S. Tonda, *Appl. Surf. Sci.*, 531 (2020) 147367.
32. S.H. Noh, M.H. Seo, J. Kang, T. Okajima, B. Han, T. Ohsaka, *NPG Asia Mater.*, 8 (2016) e312.
33. Z. Wang, X. Jin, C. Zhu, Y. Liu, H. Tan, R. Ku, Y. Zhang, L. Zhou, Z. Liu, S.J. Hwang, H.J. Fan, *Adv. Mater.*, 33 (2021) 2104718.